

Cell labeling for magnetic resonance imaging with the T_1 agent manganese chloride

Ichio Aoki,^{1,2} Yoshiyuki Takahashi,³ Kai-Hsiang Chuang,¹ Afonso C. Silva,⁴ Takehito Igarashi,³ Chuzo Tanaka,² Richard W. Childs³ and Alan P. Koretsky^{1*}

¹Laboratory of Functional and Molecular Imaging, National Institute of Neurological Disorders and Stroke, NIH, Bethesda, MD 20892-1065, USA

²Department of Medical Informatics, Meiji University of Oriental Medicine, Kyoto 629-0392, Japan

³Hematology Branch, National Heart, Lung and Blood Institute, NIH, Bethesda, MD 20892-1065, USA

⁴Cerebral Microcirculation Unit, Laboratory of Functional and Molecular Imaging, National Institute of Neurological Disorders and Stroke, NIH, Bethesda, MD 20892-1065, USA

Received 23 May 2005; Revised 31 August 2005; Accepted 24 September 2005

ABSTRACT: There is growing interest in using MRI to track cellular migration. To date, most work in this area has been performed using ultra-small particles of iron oxide. Immune cells are difficult to label with iron oxide particles. The ability of adoptively infused tumor specific T cells and N cells to traffic to the tumor microenvironment may be a critical determinant of their therapeutic efficacy. We tested the hypothesis that lymphocytes and B cells would label with $MnCl_2$ to a level that would allow their detection by T_1 -weighted MRI. Significant signal enhancement was observed in human lymphocytes after a 1 h incubation with 0.05–1.0 mM $MnCl_2$. A flow cytometry-based evaluation using propidium iodide and Annexin V staining showed that lymphocytes did not undergo apoptosis or necrosis immediately after and 24 h following a 1 h incubation with up to 1.0 mM $MnCl_2$. Importantly, NK cells and cytotoxic T cells maintained their *in vitro* killing capacity after being incubated with up to 0.5 mM $MnCl_2$. This is the first report to describe the use of $MnCl_2$ to label lymphocytes. Our data suggests $MnCl_2$ might be an alternative to iron oxide cell labeling for MRI-based cell migration studies. Copyright © 2006 John Wiley & Sons, Ltd.

KEYWORDS: manganese; cell labeling; cytotoxic T cells; NK cells; manganese-enhanced magnetic resonance imaging; apoptosis, lymphocyte

INTRODUCTION

There is rapidly growing interest in using MRI to track cell movements in animals (1,2). Most of the studies rely on labeling cells with a potent MRI contrast agent, ultra-small superparamagnetic iron oxide particles (USPIO). USPIOs create large microscopic magnetic field gradients that cause off-resonance dephasing effects which are most pronounced on T_2^* -weighted MRI (3). USPIOs

have been shown to be an excellent MRI contrast agent for detecting a wide variety of cells including endogenous macrophages (4–6) and stem cells, following *in vitro* labeling and re-implantation in animals (1,2,7). A challenge for labeling cells has been to find efficient ways to have cells accumulate USPIOs (1,2,7–9). Labeling cells with iron oxide particles provides the advantage that single cells can be detected *in vitro* and *in vivo* (10,11). A drawback of T_2^* -based contrast agents is that the agents leads to frequency shifts that lead to changes in image intensity and a number of other factors can cause frequency shifts as well affecting the specificity of detecting iron oxide-labeled cells.

A specific cell target of interest for MRI cell tracking studies has been immune cells (2). There are a wide variety of biomedical problems that would benefit from non-invasive imaging of immune cell migration. For example, the adoptive infusion of immune cells into patients with a cancer has shown promising early success. Lymphokine-activated killer cells (12), tumor-infiltrating lymphocytes, donor lymphocytes after stem cell transplantation and allogeneic natural killer (NK) cells (13) can all induce regression of a variety of cancers when

*Correspondence to: A. P. Koretsky, Laboratory of Functional and Molecular Imaging, National Institute of Neurological Disorders and Stroke, NIH, Bethesda, MD 20892, USA.

E-mail: koretskya@ninds.nih.gov

Contract/grant sponsor: Japan Society for the Promotion of Science (JSPS); Contract/grant number: 16790837.

Abbreviations used: 2D, two-dimensional; CD, cluster of differentiation; CTL, cytolytic T lymphocyte; EBV, Epstein–Barr virus; FOV, field of view; Gd-DTPA, gadolinium diethylenetriaminepentaacetic acid; HEPES, *N*-2-hydroxyethylpiperazine-*N'*-2-ethanesulfonic acid; HLA, human leukocyte antigen; IL, interleukin; LCL, lymphoblastoid cell lines; MAb, monoclonal antibody; MEMRI, manganese-enhanced magnetic resonance imaging; mHa, minor histocompatible antigen; NA, number of acquisitions; NK, natural killer; PBL, peripheral blood lymphocytes; PBMC, peripheral blood mononuclear cell; PBS, phosphate-buffered saline; PI, propidium iodide; ROI, region of interest; SE, spin-echo; ST, slice thickness; USPIO, ultra-small superparamagnetic iron oxide particles.

adoptively infused into patients. A critical determinant of the therapeutic efficacy of immune cells is the ability of these cells to traffic to the tumor microenvironment. Many MRI studies have focused on imaging immune cell migration, the majority of which used USPIO contrast. As mentioned previously, injection of USPIOs into the blood allows the detection of tissues that have accumulated macrophages (2). Lymphocytes labeled with iron oxide particles have been visualized entering the testis (14), liver, spleen (15) and pancreas of mice and rats. Lymphocytes have been successfully tracked in a mouse model of multiple sclerosis (16,17). Weissleder *et al.* reported that iron oxide-labeled NK cell could be visualized by MRI infiltrating into tumors (18). Dendritic cells have been successfully labeled with iron oxide particles using antibodies to specific receptors (19).

A shortcoming of cell tracking studies that have used USPIO is that contrast is due to off-resonance effects caused by the iron oxide. Numerous other effects can lead to off-resonance effects of comparable magnitude, including blood and susceptibility gradients around normal biological structures. Despite these shortcomings, there has been little work labeling cells with other contrast agents for MRI visualization. Johnson *et al.* reported on labeling red blood cells with gadolinium diethylenetriaminepentaacetic acid (Gd-DTPA) using an osmotic shock to enable the contrast agent to enter cells and give T_1 contrast (20). Meade and co-workers have demonstrated that fluid-phase endocytosis or direct cellular injection can be used to label cells with a variety of T_1 agents (21,22). However, endocytosis labeling tended to give better T_2^* than T_1 contrast, probably owing to high-level accumulation of the contrast agent in endosomes. Perfluorocarbon emulsions detected with ^{19}F MRI have been used to label endogenous macrophages (23) and dendritic cells via endocytosis (24). An alternative strategy would be to use a T_1 contrast agent that readily accumulates into cells.

Manganese chloride (MnCl_2) readily alters signal intensities due to changes in T_1 relaxation time on MRI, thus providing increased signal. Mn^{2+} is an essential heavy metal ion that is known to enter most cells readily. The unique biological properties of Mn^{2+} have generated renewed interest in exploring the potential of this agent as an MRI contrast agent (25). Mn^{2+} can enter cells via voltage-gated calcium channels, enabling active brain regions (26,27) and changes in inotropic status in the heart to be monitored by MRI (28). Mn^{2+} has been proposed as a cell viability indicator for cardiac applications (29). Mn^{2+} can move along neuronal pathways and this has been demonstrated to enable *in vivo* tract tracing of neuronal pathways by MRI (30,31). These observations suggest that Mn^{2+} ion can readily enter cells and will be increasingly utilized as a contrast agent for MRI-based molecular and cellular imaging.

The goal of this study was to test the hypothesis that peripheral blood lymphocytes (PBL) and Epstein–Barr virus (EBV) transformed B lymphoblastoid cell lines

(EBV-LCL) could be labeled with MnCl_2 to a level that would allow their detection by T_1 -weighted MRI. Further, we evaluated the effects of increasing Mn^{2+} concentration on the viability and function of antigen-specific cytotoxic T cells and K562-cytotoxic NK cell lines. We found that these immune cells could be labeled with Mn^{2+} at concentrations that give large changes in T_1 but have no effect on cell viability or function. Based on these findings, we conclude that *in vitro* labeling of cells with Mn^{2+} may be a useful strategy for cell tracking by MRI.

MATERIALS AND METHODS

Peripheral blood lymphocytes and lymphoblastoid cell lines

Heparinized blood samples were drawn from normal individuals ($n = 3$). PBL were obtained by density gradient centrifugation (Lymphocyte Separation Medium, ICN Biomedicals, Solon, OH, USA). Red blood cells were lysed with ACK lysing buffer (Bio Whittaker, Walkersville, MD, USA) and washed to avoid the effect of red cells on MRI. B lymphoblastoid cell lines (LCL) ($n = 1$) were established by infection of PBL with the B95-8 strain of EBV in the presence of $1\text{ }\mu\text{g/mL}$ cyclosporin A and maintained in RPMI 1640 Medium supplemented with 10% fetal calf serum, 3 mM glutamine, 100 IU/mL penicillin (RPMI/10) at 37°C in a humidified atmosphere containing 5% CO_2 and 95% air, as described (32). Manganese chloride ($\text{MnCl}_2 \cdot 4\text{H}_2\text{O}$) (Sigma, St. Louis, MO, USA) was dissolved in RPMI 1640 Medium and prepared at eight concentrations: 0 (control), 0.05, 0.1, 0.2, 0.5, 1.0, 2.0 and 5.0 mM MnCl_2 . PBL or LCL was mixed with the MnCl_2 solutions and incubated for 1 h at 37°C . Following incubation, the MnCl_2 solution was removed carefully by washing twice using RPMI 1640 Medium. After removing MnCl_2 solution from test-tubes, PBL or LCL cells were studied by flow cytometry or MRI separately. The number of cells was estimated by cell counting for each tube. There were a $\sim 24 \times 10^6$ cells per tube for MRI measurement.

Flow cytometry

LCLs were treated with MnCl_2 at a dose of 0–5.0 mM. To detect apoptotic and dead cells an Annexin V–FITC Apoptosis Detection Kit I (BD Biosciences, San Diego, CA, USA) was used. Apoptosis and necrosis were measured immediately after and 24 h after labeling with MnCl_2 . Cells were washed twice with cold PBS and resuspended in buffer at a concentration of $1 \times 10^6/\text{mL}$: 1×10^5 cells were mixed with 5 μL of fluorescein isothiocyanate (FITC)-conjugated Annexin V antibody and 5 μL of propidium iodide (PI). After 15 min of incubation at room temperature in the dark and further washes,

400 μ L of 1X binding buffer were added to each tube. Samples were analyzed within 1 h by flow cytometry (FACSCalibur, BD Immunocytometry System, San Jose, CA) and a computer station running CellQuest software. Annexin V staining was detected in the FL1 channel whereas PI staining was monitored in the FL4 channel: appropriate quadrants were set and the percentages of cells negative for both stains (viable cells), positive for Annexin V but negative for PI (apoptotic cells) and positive for PI (dead cells) were acquired.

Generation of minor histocompatibility antigen-specific T cell clones

Minor histocompatibility antigen-specific T cell lines were generated using previously-described methods (33). All peripheral blood mononuclear cells (PBMCs), T cell lines and clones were cultured in RPMI 1640 Medium supplemented with HEPES (*N*-2-hydroxyethyl-piperazine-*N'*-2-ethanesulfonic acid), 2 mM L-glutamine and 10% pooled heat-inactivated human serum. Donor T cells with reactivity for recipient minor histocompatible antigens (mHa) were generated in 24-well plates by stimulating $(1-2) \times 10^6$ PBMCs obtained from the recipient after transplantation with $(1-2) \times 10^6$ irradiated (25 Gy) PBMCs obtained from the recipient before transplantation. Cell lines were re-stimulated with irradiated recipient (pre-transplant) PBMCs at 7 and 14 days after the initial stimulation with interleukin-2-supplemented (20 U/mL) media. The resulting T cell lines were further expanded by weekly re-stimulation with irradiated EBV-transformed B cells (EBV-LCLs) derived from the recipient before transplantation. After 4–6 weeks, T cell cultures were tested for cytolytic activity against donor- and recipient-derived EBV-LCLs. T cell lines exhibiting cytolytic activity specific for recipient EBV-LCLs were cloned by limiting dilution in 96-well round-bottomed plates (0.3–0.5 cells per well) containing irradiated HLA-mismatched (allogeneic) PBMCs (5×10^4 cells per well), irradiated EBV-LCLs from the patient before transplantation (1×10^4 cells per well), recombinant human IL-2 (rhIL-2) (100 IU/mL) and anti-CD3 monoclonal antibody (MAb) (30 ng/mL). Fourteen days later, wells exhibiting cell growth were tested for target recognition by cytotoxicity. T cell clones that specifically recognized patient EBV-LCLs but not donor EBV-LCLs were further expanded for analysis of phenotype and function using anti-CD3 MAb, irradiated HLA-mismatched PBMCs and irradiated patient EBV-LCLs.

Isolation of NK cells and expansion of NK cell lines

NK cell lines were generated from peripheral blood mononuclear cells (PBMCs) as described previously

(13). PBMCs obtained from healthy donors were enriched for NK cell populations by negative depletion using immunomagnetic beads (DynaL NK cell isolation kit; Dynal Biotech, Lake Success, NY, USA) according to the manufacturer's recommended conditions. Briefly, PBMCs were incubated with an antibody mix containing anti-CD3, anti-CD14, anti-CD36, anti-CDw123 and anti-HLA class II DR/DP for 10 min at 4 °C with gentle tilting and rotation. Cells were washed with phosphate-buffered saline (PBS) 0.1% human AB serum and centrifuged for 8 min at $500 \times g$. The supernatant was discarded and the cell pellet was resuspended in PBS 0.1% human AB serum and incubated at 4 °C for 10 min after the addition of depletion Dynabeads. The cell suspension was placed in a magnetic particle concentrator (DynaL MPC; Dynal Biotech) for 2 min, the supernatant was removed and the depletion bead step was repeated. NK cell purity was determined by flow cytometry. Enriched NK cells were expanded as bulk NK populations in Cellgro SCGM serum-free medium (CellGenix, Gaithersburg, MD, USA) containing 10% pooled heat-inactivated human AB serum, 500 IU/mL of IL-2 and irradiated (100 Gy) allogeneic EBV-LCLs as feeder cells (1000:1 EBV-LCL:NK cell ratio). Two weeks after expansion, bulk NK cells were stained with anti-CD56 Cy-chrome and were then sorted using a MoFlo flow cytometer (DAKO-Cytomation, Fort Collins, CO, USA) to isolate CD56⁺ populations that were re-expanded for 2 weeks using the same condition as described above and used for cytotoxicity assays.

Cytotoxicity assays

Cytotoxicity assays were performed using ^{51}Cr release as described previously (33). Briefly, target cells were labeled for 2 h with ^{51}Cr (100 μCi (3.7 MBq) per 10^6 cells), washed and then re-suspended at a concentration of $1 \times 10^5/\text{mL}$; 100 μL of each target (in replicates of two) were co-cultured with various numbers of effector cells (100 μL) in 96-well round-bottomed plates (total volume 200 μL). After incubating at 37 °C for 4 h, 100 μL of supernatant were harvested for gamma counting. The percentage of specific lysis was calculated using the equation $100 \times (\text{cpm released from test sample} - \text{cpm spontaneous release}) / (\text{cpm maximum release} - \text{cpm spontaneous release})$. All values used represented the average of both replicates.

MRI measurements

MRI measurements were performed on cells incubated with different MnCl_2 concentrations consisting of 0, 0.05, 0.1, 0.2, 1.0, 2.0 and 5.0 mM both for PBL ($n = 3$) and LCL ($n = 1$). Cells ($\sim 24 \times 10^6$) were put into 0.2 mL PCR tubes and imaged after settling into a pellet by gravity. The MRI acquisitions were performed

in an 11.7 T, 31 cm bore magnet (Magnex Scientific, Yarnton, UK) interfaced to a Bruker Avance console (Bruker Medical, Ettlingen, Germany) 2 h after cell preparation. One PBL sample consisting of eight tubes was also measured 6, 12, 18 and 24 h after labeling. A 27 mm diameter birdcage coil (Bruker Medical) was used for measurement of cell samples. The different PCR tubes were mounted on a plastic holder having 2×4 holes and set in the center of the birdcage coil. The sample temperature was maintained at room temperature ($\sim 23^\circ\text{C}$). The measurements were performed in the following order: T_1 -weighted imaging using conventional spin echo (SE) sequence, multi-echo SE imaging for T_2 calculations and inversion–recovery SE imaging for T_1 calculations.

T_1 -weighted imaging. Three sets of two-dimensional (2D), multi-slice, T_1 -weighted images were obtained using a conventional SE sequence with the following parameters: pulse repetition time (TR) = 300 ms; echo time (TE) = 7.54 ms; matrix size = 256×256 for coronal slice, 128×256 for horizontal and sagittal slices; field of view (FOV) = 19.2×19.2 mm for coronal slice, 19.2×9.6 mm for horizontal and sagittal slices; slice thickness (ST) = 1 mm; and number of acquisitions (NA) = 24. Slice orientation was coronal (four slices with 9 mm slice offset), horizontal (two slices with 2 mm slice offset) and sagittal (two slices with 9 mm slice offset). For these images, the nominal voxel resolution was $75 \times 75 \times 1000 \mu\text{m}$. The total acquisition time for three slices was 61.4 min.

Multi-echo imaging. 2D multi-slice multi-echo imaging was performed to generate T_2 maps with the following parameters: TR = 12 000 ms, TE = 10, 20, 30, 40, 50, 60, 70 and 80 ms, number of echoes = 8, matrix size = 128×128 , slice orientation = coronal (same slice orientation as T_1 -weighted imaging), FOV = 19.2×19.2 mm, ST = 1 mm and NA = 2. For these images, the nominal voxel resolution was $150 \times 150 \times 1000 \mu\text{m}$. The total acquisition time for multi-echo imaging was 51.2 min.

Inversion–recovery. 2D multi-slice inversion–recovery MRI was carried out using a spin-echo acquisition for T_1 map calculation with the following parameters: TR = 16 000 ms, TE = 5.7 ms, inversion time = 10, 300, 600, 1000, 1500, 2000, 3000, 4000 ms, matrix size = 128×128 , slice orientation = coronal (same slice orientation as T_1 -weighted imaging), FOV = 19.2×19.2 mm, ST = 1 mm and NA = 1. For these images, the nominal voxel resolution was $150 \times 150 \times 1000 \mu\text{m}$. The total acquisition time for inversion–recovery MRI was 4.6 h.

Data analysis and statistical analysis

Quantitative T_1 maps were calculated by a non-linear least-squares fitting using inversion–recovery MRI. In

addition, quantitative T_2 maps were calculated by a non-linear least-squares fitting using multi-echo imaging. Regions of interest (ROI) were defined as precipitated cell regions and clear supernatant liquid. All calculations and analyses were performed using Matlab (Version 6.5) (MathWorks, Natick, MA, USA), MRVision image analysis software (Version 1.5.8) (MRVision, Winchester, MA, USA) on Linux PC (Red Hat Linux, Raleigh, CA, USA) and Macintosh (Mac OS X, Version 10.2) (Apple Computer, Cupertino, CA, USA). All data are presented as means \pm SD. All statistical analyses were performed using StatView (Version 5.0) (SAS Institute, Cary, NC, USA). A probability value of < 0.05 was considered significant for each analysis.

RESULTS

T_1 and T_2 relaxation time shortening due to cell labeling with MnCl_2

Figure 1(A) shows typical T_1 -weighted images of pelleted manganese-labeled human lymphocytes. Signal enhancement after labeling with concentrations that varied from 0.05 to 1.0 mM MnCl_2 in the media was observed in human lymphocytes in comparison with the controls. A signal loss for incubation concentrations of over 2.0 mM was observed owing to shortening of the T_2 relaxation time. Typical calculated maps of T_1 [Fig. 1(B)] and T_2 [Fig. 1(C)] of the manganese-labeled human lymphocytes and the values of T_1 [Fig. 1(D)] and T_2 [Fig. 1(E)] are shown. The T_1 and T_2 relaxation times changed depending on the manganese concentration. There was a peak of signal intensity in T_1 -weighted imaging for the parameters used for incubation concentrations of 0.5–1.0 mM MnCl_2 .

T_1 relaxation times of the medium were not significantly affected in controls or cells labeled with up to 2.0 mM MnCl_2 . T_1 for the medium was shortened at the 2.0 and 5.0 mM concentrations, indicating that there was significant manganese release from cells or significant cell death as a consequence of high MnCl_2 concentrations. Indeed, Mn^{2+} release from pre-loaded cells may be an MRI approach to monitoring apoptosis.

The retention time of the contrast elicited by MnCl_2 in labeled cells was measured for the time period from 0 to 24 h after MnCl_2 labeling. Typical T_1 -weighted images of pelleted human lymphocytes at 2 h after labeling [Fig. 2(A)] and 24 h after labeling [Fig. 2(B)] are shown. Signal enhancement on T_1 -weighted images was still observed 24 h after MnCl_2 labeling at all manganese concentrations except for the control and the 5.0 mM concentration. Figure 2(C) and (D) show graphs of the change in T_1 and T_2 , respectively, from 0 to 24 h after the MnCl_2 labeling. Both T_1 and T_2 increased slightly over 24 h except for control cells and cells labeled with 2.0 mM MnCl_2 .

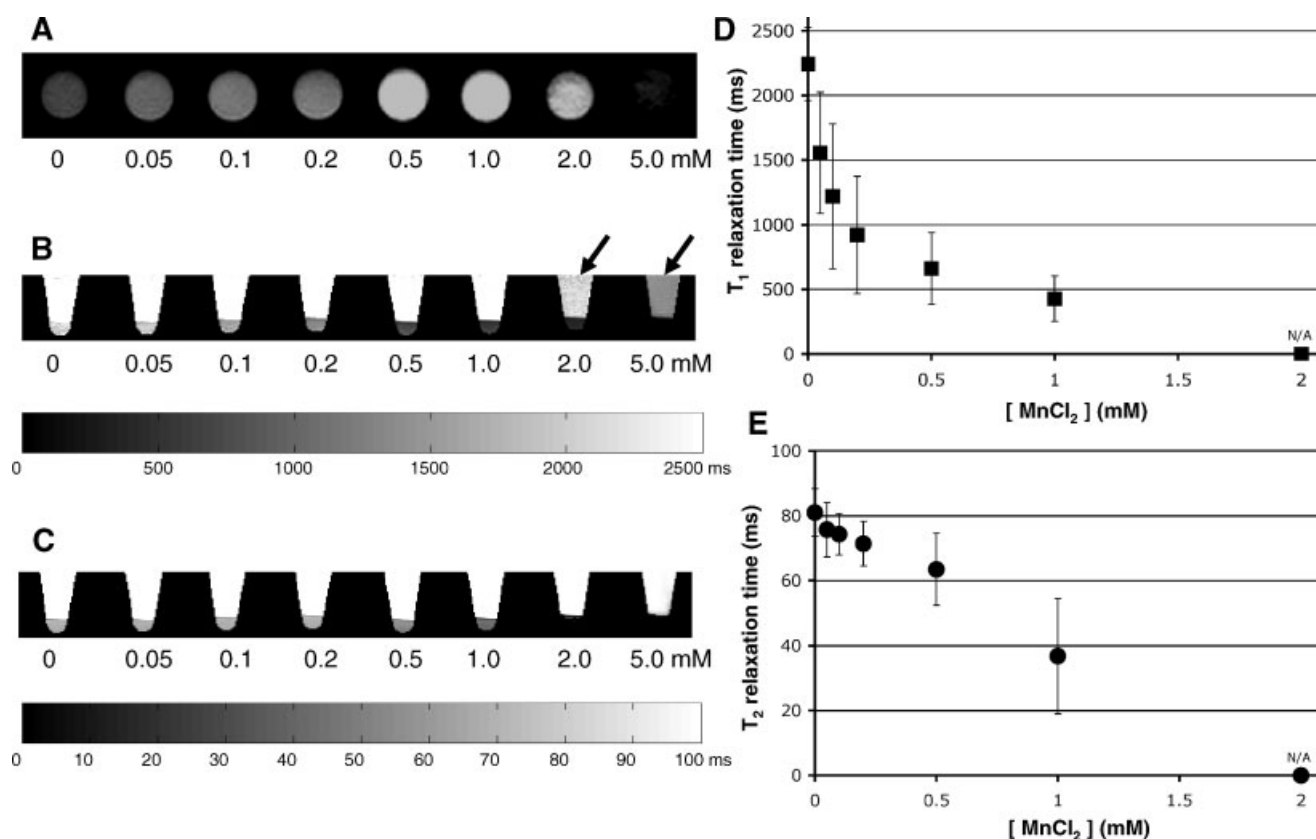


Figure 1. T_1 and T_2 relaxation times relative to manganese concentration in pelleted human lymphocytes. (A) Typical T_1 -weighted images of pelleted manganese-labeled human lymphocytes. The images were acquired in the horizontal plane using a conventional spin-echo sequence. There were $\sim 24 \times 10^6$ cells per tube ($n = 3$). Signal enhancement from 0.05 to 1.0 mM was observed in human lymphocytes compared with controls (0 mM). A signal loss with concentrations > 2.0 mM was observed due to shortening of the T_2 relaxation time. Typical calculated maps of T_1 (B) and T_2 (C) relaxation times of the pelleted manganese-labeled human lymphocytes and the values of T_1 (D) and T_2 (E) are shown. Raw data were acquired in the vertical plane using the inversion-recovery spin-echo sequence for T_1 maps and multi-echo spin-echo sequence for T_2 maps. T_1 and T_2 relaxation times showed exponential and linear attenuation depending on the manganese concentration, respectively. Note that T_1 relaxation times of the medium (arrows) were shortened at the 2.0 and 5.0 mM concentrations owing to release and/or disruption of lymphocytes

Propidium iodide and Annexin V staining to test for cell viability

Figure 3(A) shows the results of the flow cytometry after staining human EBV-LCL with propidium iodide (PI), a vital dye that stains necrotic and or apoptotic cells. Significant numbers of PI-positive cells were observed only after labeling with doses of ≥ 2.0 mM MnCl_2 . Figure 3(B) shows flow cytometry staining with Annexin V used to detect cells undergoing apoptotic death. Significant numbers of Annexin V-positive cells were observed only after labeling with doses of > 2.0 mM MnCl_2 . By comparing the PI and Annexin V results, the number of total dead cells and cells destined for apoptotic death were determined. Figure 3(C) shows the percentage of total dead cells that were positive for both PI and Annexin V. Compared with controls, cell viability decreased only at the 2.0 and 5.0 mM MnCl_2 concentrations (Bonferroni/Dunn, $*P < 0.05$). Figure 3(D) shows the percentage of cells undergoing apoptosis (PI negative

and Annexin V positive). Compared with controls, an increase in apoptotic cells was only observed at the 5.0 mM MnCl_2 concentration (Bonferroni/Dunn, $*P < 0.05$). No cellular apoptosis or necrosis was observed with labeling for 1 h up to a 1.0 mM MnCl_2 concentration. Necrotic cells were also measured by cell counting after Trypan Blue staining (Table 1). Compared with controls, the percentage of necrotic human lymphocytes increased significantly at the 2.0 and 5.0 mM MnCl_2 concentrations 24 h after labeling (Dunnnett, $*P < 0.05$).

Chromium-51 release assay study

Figure 4 shows the chromium-51 (^{51}Cr) release assay for NK cells targeting the NK cell-sensitive leukemia cell line K562, (A) 2 h and (B) 24 h after labeling NK cells with MnCl_2 . Also shown are the cytotoxic potential of an mHa specific T lymphocyte (CTL) clone against EBV-LCL that express the target mHa 2 h [Fig. 4(C)]

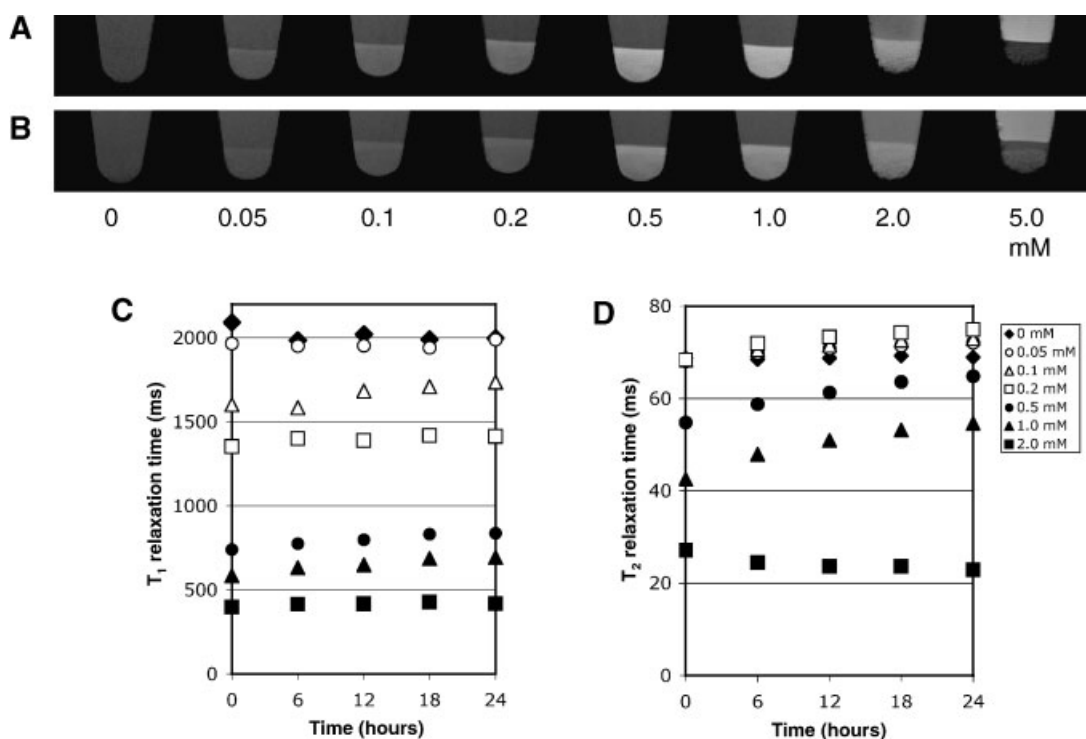


Figure 2. Changes in T_1 and T_2 relaxation times in human lymphocytes 0–24 h after manganese cell labeling. Typical vertical sliced of T_1 -weighted images of pelleted human lymphocytes 2 h (A) and 24 h (B) after $MnCl_2$ suspension. Signal enhancement on T_1 -weighted images continued 24 h after $MnCl_2$ labeling at all manganese concentrations except for the control and 5.0 mM concentration. Graphs show the change in T_1 (C) and T_2 (D) relaxation time from 0 to 24 h after $MnCl_2$ labeling ($n = 1$). Filled diamond, open circle, open triangle, open square, filled circle, filled triangle and filled square indicate control (0 mM), 0.05, 0.1, 0.2, 0.5, 1.0 and 2.0 mM concentrations, respectively. Both T_1 and T_2 relaxation times increased slightly over 24 h with the exception of the control and 2.0 mM concentration

and 24 h [Fig. 4(D)] after $MnCl_2$ labeling of the CTL. NK cell function [Fig. 4(A) and (B)] and CTL function [Fig. 4(C) and (D)] after labeling effector cells with $MnCl_2$ (0–0.5 mM) for 1 h are shown. There was no significant difference between control and $MnCl_2$ -labeled cells up to 0.5 mM (Bonferroni/Dunn, $*P < 0.05$).

Manganese cell labeling for different cell types.

Figure 5 shows typical T_1 -weighted images of immortalized human EBV-LCL 2 h after $MnCl_2$ labeling; compared with controls, signal enhancement from 0.05 to 0.5 mM was observed. A signal loss occurred with $MnCl_2$ concentrations > 2.0 mM due to shortening of the T_2 relaxation time. The signal intensity of the medium was enhanced at the 2.0 and 5.0 mM concentrations, possibly owing to spontaneous manganese release or the higher manganese concentration causing disruption of the human B cells. The results observed with the immortalized B cell line were consistent with similar experiments conducted on freshly isolated human lymphocytes (Fig. 1).

DISCUSSION

There have been just a few preliminary reports of the use of $MnCl_2$ to label cells *in vitro* for MRI (34,35). This is the first report to describe the use of $MnCl_2$ to label lymphocytes to a level sufficient for their detection by MRI. There were no toxic effects 24 h after labeling cells for 1 h with up to 0.5 mM $MnCl_2$. There were three major findings in this study: (1) significant signal enhancement was observed in normal human peripheral blood lymphocytes and EBV-LCL B lymphocytes at both 2 and 24 h after incubation with 0.05–1.0 mM $MnCl_2$ on T_1 -weighted MRI. In addition, both T_1 and T_2 relaxation times decreased significantly depending on the concentration of $MnCl_2$ used for labeling, although T_1 decreased more rapidly at lower doses. These results indicate that $MnCl_2$ allowed MRI cell visualization by functioning as a T_1 contrast agent. (2) No apoptosis or necrosis of human lymphocytes was observed using up to 1.0 mM $MnCl_2$. (3) The killer activity of both NK cells and cytotoxic T cells was not significantly affected up to 0.5 mM $MnCl_2$.

Labeling isolated cells *in vitro* with dextran-coated iron oxide particles has been successfully used to track by MRI a wide variety of cells introduced into animals

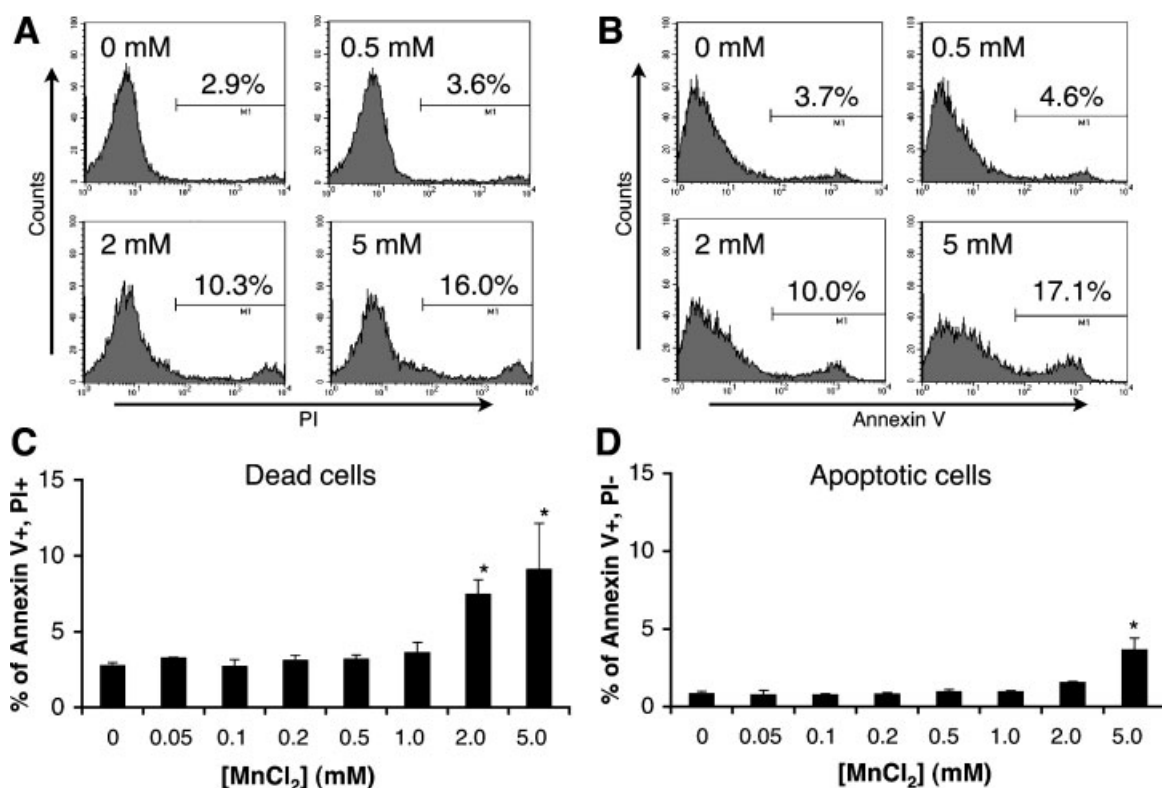


Figure 3. Cell viability after suspension in MnCl₂ evaluated using propidium iodide (PI) and Annexin V. (A) Flow cytometry results after staining EBV lymphoblastoid cell lines with PI. PI is a vital dye that stains necrotic cells. PI-positive cells were observed when the manganese concentration was increased to >2.0 mM (at 1 h). (B) Flow cytometry results after staining with Annexin V. Annexin V positivity is consistent with cells being either apoptotic or necrotic. Annexin V positivity occurred when the manganese concentration was increased to >2.0 mM (at 1 h). (C) Percentage of dead cells (both PI positive and Annexin V positive). Dead cells increased significantly at the 2.0 and 5.0 mM MnCl₂ concentrations compared with controls (**P* < 0.05). (D) Percentage of apoptotic cells (PI negative and Annexin V positive). Apoptotic cells increased significantly at the 5.0 mM MnCl₂ concentration compared with controls (**P* < 0.05). No apoptosis or necrosis in lymphocytes occurred up to a concentration of 1.0 mM MnCl₂ (1 h suspension)

Table 1. Cell viability of human lymphocytes after suspension of MnCl₂ evaluated by cell counting using Trypan Blue staining^a

MnCl ₂ concentration ratio of necrotic cells to the control ^b		
(mM)	0 h after suspension	24 h after suspension
0 (control)	1.00 ± 0.17	1.00 ± 0.13
0.05	0.88 ± 0.13	0.97 ± 0.18
0.1	1.07 ± 0.21	0.91 ± 0.06
0.2	0.89 ± 0.10	1.07 ± 0.11
0.5	0.92 ± 0.12	0.91 ± 0.14
1.0	0.84 ± 0.13	0.96 ± 0.16
2.0	0.81 ± 0.10	0.72 ± 0.18 ^c
5.0	0.64 ± 0.09 ^c	0.23 ± 0.08 ^c

^aResults of the cell counting after staining human lymphocytes with Trypan Blue. Trypan Blue is a vital dye that stains necrotic cells. A significant increase in the % of Trypan Blue-positive cells was observed immediately following a 1 h incubation in 5.0 mM MnCl₂ and 24 h following a 1 h incubation in 2.0 mM MnCl₂ (Dunnett, **P* < 0.05). No lymphocyte necrosis was observed up to a concentration of 1.0 mM MnCl₂ after a 1 h suspension.

^bMean ± SE.

^cStatistically significant in comparison with each of controls. Dunnett, *P* < 0.05.

(1,2,7). The use of MRI to study cell migration in animal models is growing rapidly and is expected to impact a variety of fields such as *in vivo* evaluation of transplantation, regeneration and cell therapy. Iron oxide particles have very high sensitivity on T₂*-weighted MRI. Indeed, both *in vitro* and *in vivo* it has been demonstrated that a single iron oxide-loaded cell can be detected by MRI (11). A drawback of cell labeling using iron oxide particles is that T₂* effects lead to decrease in signal intensity, creating a need for homogeneous images. Another drawback is that specialized techniques are required to achieve sufficient labeling with iron oxide such as catalyzing endocytosis with lipofection agents, peptides or cell receptor antibodies (1,2,7).

MnCl₂ may offer several advantages that could overcome these problems. Because MnCl₂ shortens T₁ relaxation times, it produces positive signal enhancement on T₁-weighted MRI. In addition, the labeling technique with MnCl₂ is very simple, only requiring incubation for a relatively short period of time. The simple strategy of incubating cells with MnCl₂ used on lymphocytes in these experiments should be widely applicable to other

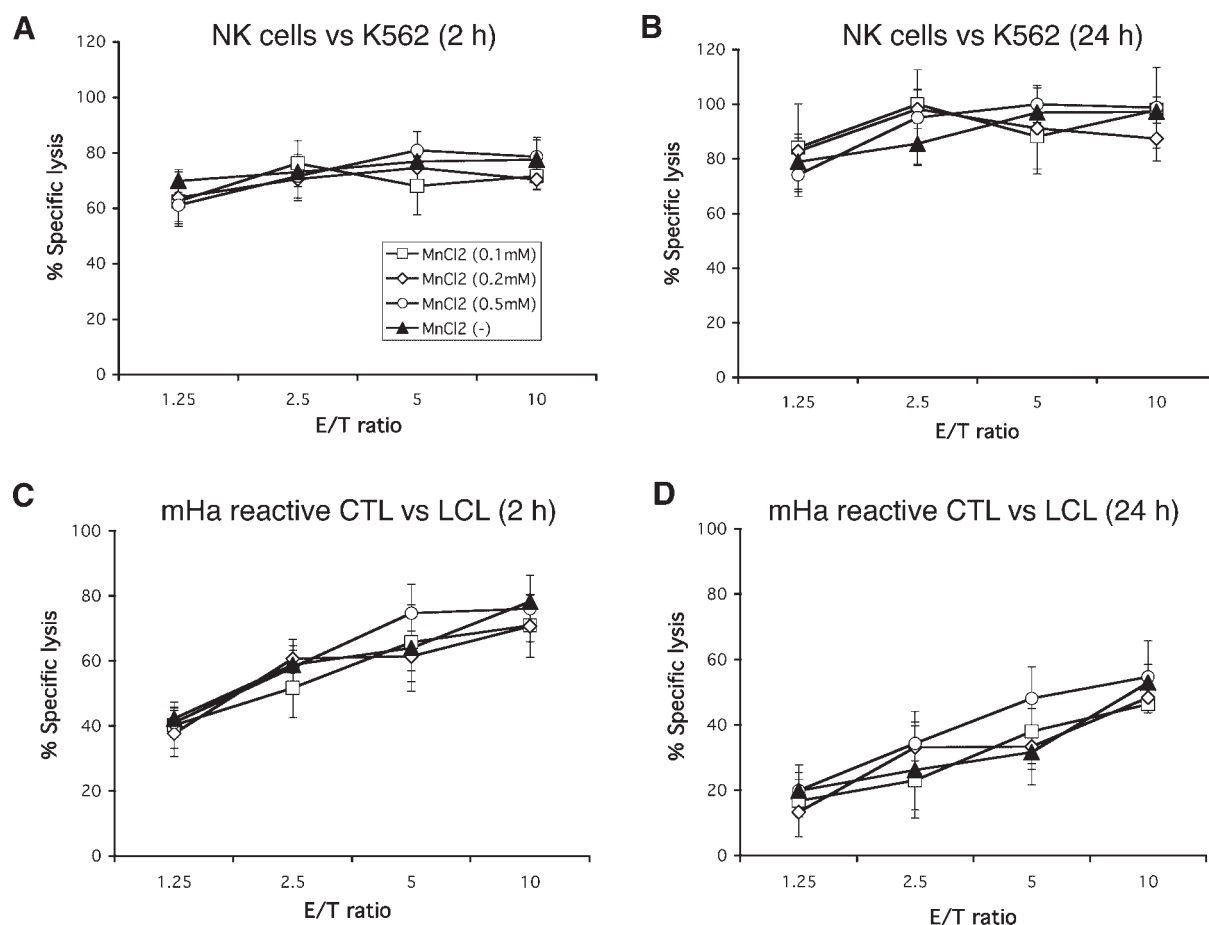


Figure 4. Chromium-51 cytotoxicity release assay 2 and 24 h following manganese labeling. NK cell function assessed by ^{51}Cr release assay for NK cells against K562 cells 2 h (A) and 24 h (B) after manganese labeling at various concentrations. Killer T cell function assessed by ^{51}Cr release assay for an mHa-reactive CTL clone against B LCL 2 h (C) and 24 h (D) after manganese labeling at various concentrations. There was no significant difference between controls and manganese labeled cells up to the 0.5 mM manganese concentration ($*P < 0.05$). This suggests that the killer activity of both NK cells and cytotoxic T cells was not significantly affected up to 0.5 mM MnCl_2 . E/T: effector/target

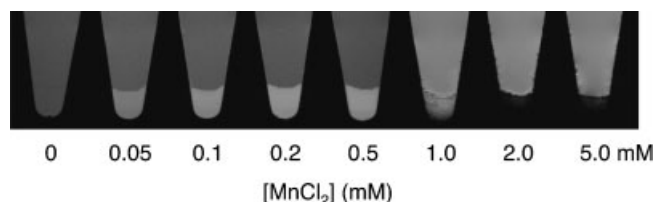


Figure 5. T_1 -weighted MRI of pellet immortalized human B cells 2 h after MnCl_2 labeling (for 1 h). Typical T_1 -weighted images of immortalized B lymphoblastoid cell lines 2 h after suspension in various concentrations of MnCl_2 for 1 h. The images were acquired in a vertical plane using conventional spin-echo sequences. Signal enhancement was observed with MnCl_2 manganese concentrations ranging from 0.05 to 0.5 mM. A signal loss occurred with concentrations > 2.0 mM due to shortening of the T_2 relaxation time. The signal intensity of the medium was enhanced at concentrations from 2.0 to 5.0 mM owing to spontaneous release and/or to disruption of B cells

cell types, as it has already been established that the manganese ion can be efficiently taken up into a number of different cells through a variety of mechanisms. In combination with iron oxide, it should be possible to double label cells.

A potential drawback with Mn^{2+} for cell labeling is the need to avoid cellular toxicities that may be associated with this element. Like other heavy metals, manganese is essential for cell viability at normal levels but can be toxic at higher concentrations. It is known that high levels of chronic manganese exposure causes symptoms of 'manganism' associated with extrapyramidal motor system dysfunction presenting with a clinical picture similar to Parkinson's disease (36). In general, manganese toxicity requires prolonged exposure times. In contrast, there are no reports of toxicity when exposure to manganese is limited to 1 h or less. No toxic effects for viability of PC12 cells 24 and 48 h after incubation with 0.2 mM MnCl_2 (37) and 24 h with 0.5 mM MnCl_2 (38) have been reported. Our observation that *in vitro*

concentrations of $\text{Mn}^{2+} \geq 2 \text{ mM}$ were toxic whereas lower doses were safe is consistent with a previous report showing that ATP-dependent Ca^{2+} transport is inhibited by 1.8 mM Mn^{2+} but supported by 0.3 mM Mn^{2+} in the rat brain synaptosome (39). A critical balance is needed to optimize the MnCl_2 concentration for MRI labeling that will be both effective and non-toxic to the cells. Here we have demonstrated that this balance can be achieved in human lymphocytes. Cell labeling for 1 h with $0.5\text{--}1.0 \text{ mM MnCl}_2$ gave the largest signal enhancement on T_1 -weighted MRI at 11.7 T without causing significant cytotoxic effects. Importantly, the baseline cytotoxic function of both NK cells and CTL were maintained for at least 1 day after labeling for 1 h at the 0.5 mM MnCl_2 concentration. These results indicate that (1) cells labeled with MnCl_2 maintain their immunological function and (2) the optimal and safe concentration of MnCl_2 for cell labeling in human lymphocytes is $\sim 0.5 \text{ mM}$.

Another question regarding MnCl_2 labeling of cells is how long they will retain the increased Mn^{2+} . The wash-out of Mn^{2+} from labeled cells was slow during the first 24 h. Preliminary research indicated that contrast is high 48 h after labeling (data not shown). In these experiments, labeled cells were washed with medium twice then suspended in medium without MnCl_2 for 2 or 24 h. It is generally considered that MRI-detectable Mn^{2+} arises from intracellular sources, and our results are consistent with this concept (40). It has been demonstrated that there are multiple routes for Mn^{2+} entry into cells, including calcium channels (41) and via endocytosis (42) and specific heavy metal transporters (43). The slow excretion of manganese is consistent with there being an absence of known Mn^{2+} exporters. Systemic administration of manganese in rats led to signal enhancement in the brain detectable by MRI for up to 14 days (44).

Another shortcoming is the sensitivity of MRI to MnCl_2 -labeled cells. From one to a few cells can be detected when labeled with iron oxide (15,18). Based on the large T_1 changes measured in the cell pellets, we estimate that $5\text{--}10\%$ of the cells ($\sim 50\text{--}100$ cells in a $100 \mu\text{m}^3$ voxel) should be detectable. Although this is a much larger cell number than detectable with iron oxide, it may still prove useful in a variety of experimental protocols.

In conclusion, we have shown that significant changes in T_1 -weighted MRI signal intensity can be achieved in human lymphocytes with a short incubation of MnCl_2 at concentrations that do not have deleterious effects on cellular viability or function. The contrast change detected lasted for at least 24 h and raises the possibility that MnCl_2 labeling of lymphocytes could be used to track these cells into tumors and other tissues using high spatial resolution MRI. MnCl_2 may offer advantages over the more widely used approach of labeling cells with iron oxide, including ease of labeling and improved signal enhancement on MRI.

Acknowledgements

The authors thank Drs J. Philip McCoy, Jr (National Heart, Lung and Blood Institute, NIH), Erik M. Shapiro (Laboratory of Functional and Molecular Imaging, NINDS, NIH), Akihiro Tomita (Nagoya University, Japan), Keiichi Koizumi and Tsugunobu Ando (Toyama Medical and Pharmaceutical University, Japan) and Toshihiro Higuchi and Masahiro Umeda (Meiji University of Oriental Medicine) for valuable discussions. This work was partly supported by Grants-in-Aid for Scientific Research (Kakenhi, No. 16790837) of the Japan Society for the Promotion of Science (JSPS).

REFERENCES

- Bulte JW, Kraitchman DL. Monitoring cell therapy using iron oxide MR contrast agents. *Curr. Pharm. Biotechnol.* 2004; **5**: 567–584.
- Ho C, Hitchens TK. A non-invasive approach to detecting organ rejection by MRI: monitoring the accumulation of immune cells at the transplanted organ. *Curr. Pharm. Biotechnol.* 2004; **5**: 551–566.
- Bulte JW, Brooks RA. Magnetic nanoparticles as contrast agents for MR imaging. In *Scientific and Clinical Applications of Magnetic Carriers*, Häfeli U, Schütt W, Teller J, Zborowski M (eds). Plenum Press: New York, 1997; 527–543.
- Weissleder R, Stark DD, Engelstad BL, Bacon BR, Compton CC, White DL, Jacobs P, Lewis J. Superparamagnetic iron oxide: pharmacokinetics and toxicity. *AJR Am. J. Roentgenol.* 1989; **152**: 167–173.
- Doerfler A, Engelhorn T, Heiland S, Knauth M, Wanke I, Forsting M. MR contrast agents in acute experimental cerebral ischemia: potential adverse impacts on neurologic outcome and infarction size. *J. Magn. Reson. Imaging* 2000; **11**: 418–424.
- Kanno S, Lee PC, Dodd SJ, Williams M, Griffith BP, Ho C. A novel approach with magnetic resonance imaging used for the detection of lung allograft rejection. *J Thorac. Cardiovasc. Surg.* 2000; **120**: 923–934.
- Bulte JW, Arbab AS, Douglas T, Frank JA. Preparation of magnetically labeled cells for cell tracking by magnetic resonance imaging. *Methods Enzymol.* 2004; **386**: 275–299.
- Hinds KA, Hill JM, Shapiro EM, Laukkanen MO, Silva AC, Combs CA, Varney TR, Balaban RS, Koretsky AP, Dunbar CE. Highly efficient endosomal labeling of progenitor and stem cells with large magnetic particles allows magnetic resonance imaging of single cells. *Blood* 2003; **102**: 867–872.
- Shapiro EM, Skrtic S, Sharer K, Hill JM, Dunbar CE, Koretsky AP. MRI detection of single particles for cellular imaging. *Proc. Natl. Acad. Sci. USA* 2004; **101**: 10901–10906.
- Dodd SJ, Williams M, Suhan JP, Williams DS, Koretsky AP, Ho C. Detection of single mammalian cells by high-resolution magnetic resonance imaging. *Biophys. J.* 1999; **76**: 103–109.
- Shapiro EM, Sharer K, Skrtic S, Koretsky AP. *In vivo* detection of single cells by MRI. *Magn. Reson. Med.* 2005; in press.
- Rosenberg SA, Lotze MT, Muul LM, Chang AE, Avis FP, Leitman S, Linehan WM, Robertson CN, Lee RE, Rubin JT, Seipp CA, Simpson CG, White DE. A progress report on the treatment of 157 patients with advanced cancer using lymphokine-activated killer cells and interleukin-2 or high-dose interleukin-2 alone. *N. Engl. J. Med.* 1987; **316**: 889–897.
- Igarashi T, Wynberg J, Srinivasan R, Becknell B, McCoy JP Jr, Takahashi Y, Suffredini DA, Linehan WM, Caligiuri MA, Childs RW. Enhanced cytotoxicity of allogeneic NK cells with killer immunoglobulin-like receptor ligand incompatibility against melanoma and renal cell carcinoma cells. *Blood* 2004; **104**: 170–177.
- Yeh TC, Zhang W, Ildstad ST, Ho C. Intracellular labeling of T cells with superparamagnetic contrast agents. *Magn. Reson. Med.* 1993; **30**: 617–625.

15. Dodd CH, Hsu HC, Chu WJ, Yang P, Zhang HG, Mountz JD Jr, Zinn K, Forder J, Josephson L, Weissleder R, Mountz JM, Mountz JD. Normal T cell response and *in vivo* magnetic resonance imaging of T cells loaded with HIV transactivator-peptide-derived superparamagnetic nanoparticles. *J. Immunol. Methods* 2001; **256**: 89–105.
16. Moore A, Sun PZ, Cory D, Hogemann D, Weissleder R, Lipes MA. MRI of insulinitis in autoimmune diabetes. *Magn. Reson. Med.* 2002; **47**: 751–758.
17. Anderson SA, Shukaliak-Quandt J, Jordan EK, Arbab AS, Martin R, McFarland H, Frank JA. Magnetic resonance imaging of labeled T cells in a mouse model of multiple sclerosis. *Ann. Neurol.* 2004; **55**: 654–659.
18. Weissleder R, Cheng HC, Bogdanova A, Bogdanov A, Jr. Magnetically labeled cells can be detected by MR imaging. *J. Magn. Reson. Imaging* 1997; **7**: 258–263.
19. Ahrens ET, Feili-Hariri M, Xu H, Genove G, Morel PA. Receptor-mediated endocytosis of iron-oxide particles provides efficient labeling of dendritic cells for *in vivo* MR imaging. *Magn. Reson. Med.* 2003; **49**: 1006–1013.
20. Johnson KM, Tao JZ, Kennan RP, Gore JC. Gadolinium-bearing red cells as blood pool MRI contrast agents. *Magn. Reson. Med.* 1998; **40**: 133–142.
21. Li WH, Parigi G, Fragai M, Luchinat C, Meade TJ. Mechanistic studies of a calcium-dependent MRI contrast agent. *Inorg. Chem.* 2002; **41**: 4018–4024.
22. Modo M, Cash D, Mellodew K, Williams SC, Fraser SE, Meade TJ, Price J, Hodges H. Tracking transplanted stem cell migration using bifunctional, contrast agent-enhanced, magnetic resonance imaging. *Neuroimage* 2002; **17**: 803–811.
23. Mason RP, Antich PP, Babcock EE, Gerberich JL, Nunnally RL. Perfluorocarbon imaging *in vivo*: a ^{19}F MRI study in tumor-bearing mice. *Magn. Reson. Imaging* 1989; **7**: 475–485.
24. Ahrens ET, Flores R, Xu H, Morel PA. *In vivo* imaging platform for tracking immunotherapeutic cells. *Nat. Biotechnol.* 2005; **23**: 983–987.
25. Koretsky AP, Silva AC. Manganese-enhanced magnetic resonance imaging (MEMRI). *NMR Biomed.* 2004; **17**: 527–531.
26. Lin YJ, Koretsky AP. Manganese ion enhances T_1 -weighted MRI during brain activation: an approach to direct imaging of brain function. *Magn. Reson. Med.* 1997; **38**: 378–388.
27. Aoki I, Tanaka C, Takegami T, Ebisu T, Umeda M, Fukunaga M, Fukuda K, Silva AC, Koretsky AP, Naruse S. Dynamic activity-induced manganese-dependent contrast magnetic resonance imaging (DAIM MRI). *Magn. Reson. Med.* 2002; **48**: 927–933.
28. Hu TC, Pautler RG, MacGowan GA, Koretsky AP. Manganese-enhanced MRI of mouse heart during changes in inotropy. *Magn. Reson. Med.* 2001; **46**: 884–890.
29. Brurok H, Skoglund T, Berg K, Skarra S, Karlsson JO, Jynge P. Myocardial manganese elevation and proton relaxivity enhancement with manganese dipyrroxyl diphosphate. *Ex vivo* assessments in normally perfused and ischemic guinea pig hearts. *NMR Biomed.* 1999; **12**: 364–372.
30. Pautler RG, Silva AC, Koretsky AP. *In vivo* neuronal tract tracing using manganese-enhanced magnetic resonance imaging. *Magn. Reson. Med.* 1998; **40**: 740–748.
31. Van der Linden A, Verhoye M, Van Meir V, Tindemans I, Eens M, Absil P, Balthazart J. *In vivo* manganese-enhanced magnetic resonance imaging reveals connections and functional properties of the songbird vocal control system. *Neuroscience* 2002; **112**: 467–474.
32. Khanolkar A, Fu Z, Underwood LJ, Bondurant KL, Rochford R, Cannon MJ. CD4⁺ T cell-induced differentiation of EBV-transformed lymphoblastoid cells is associated with diminished recognition by EBV-specific CD8⁺ cytotoxic T cells. *J. Immunol.* 2003; **170**: 3187–3194.
33. Takahashi Y, McCoy JP Jr, Carvallo C, Rivera C, Igarashi T, Srinivasan R, Young NS, Childs RW. *In vitro* and *in vivo* evidence of PNH cell sensitivity to immune attack after nonmyeloablative allogeneic hematopoietic cell transplantation. *Blood* 2004; **103**: 1383–1390.
34. Aoki I, Takahashi Y, Chuang K, Igarashi T, Silva AC, Tanaka C, Childs RW, Koretsky AP. *In vitro* cell labeling for manganese enhanced magnetic resonance imaging. In *Proceedings of the Twelfth Scientific Meeting and Exhibition of the International Society for Magnetic Resonance in Medicine (ISMRM)*, Kyoto, Japan, 2004. ISMRM: 2004; 164.
35. Gimi B, Leoni L, Desai T, Magin RL, Roman BB. Imaging of pancreatic beta cell function by Mn^{2+} -enhanced MRI. In *Proceedings of the Tenth Scientific Meeting and Exhibition of the International Society for Magnetic Resonance in Medicine (ISMRM)*, Honolulu, Hawaii, 2002. ISMRM: 2002; 567.
36. Barbeau A. Manganese and extrapyramidal disorders (a critical review and tribute to Dr George C. Cotzias). *Neurotoxicology* 1984; **5**: 13–35.
37. Migheli R, Godani C, Sciola L, Delogu MR, Serra PA, Zangani D, De Natale G, Miele E, Desole MS. Enhancing effect of manganese on L-DOPA-induced apoptosis in PC12 cells: role of oxidative stress. *J. Neurochem.* 1999; **73**: 1155–1163.
38. Desole MS, Sciola L, Delogu MR, Sircana S, Migheli R. Manganese and 1-methyl-4-(2'-ethylphenyl)-1,2,3,6-tetrahydropyridine induce apoptosis in PC12 cells. *Neurosci. Lett.* 1996; **209**: 193–196.
39. Low W, Brawarnick N, Rahamimoff H. The inhibitory effect of Mn^{2+} on the ATP-dependent Ca^{2+} pump in rat brain synaptic plasma membrane vesicles. *Biochem. Pharmacol.* 1991; **42**: 1537–1543.
40. Koretsky AP. Functional assessment of tissues with magnetic resonance imaging. *Ann. N. Y. Acad. Sci.* 2002; **961**: 203–205.
41. Narita K, Kawasaki F, Kita H. Mn and Mg influxes through Ca channels of motor nerve terminals are prevented by verapamil in frogs. *Brain Res.* 1990; **510**: 289–295.
42. Suarez N, Eriksson H. Receptor-mediated endocytosis of a manganese complex of transferrin into neuroblastoma (SHSY5Y) cells in culture. *J. Neurochem.* 1993; **61**: 127–131.
43. Durr G, Strayle J, Plemper R, Elbs S, Klee SK, Catty P, Wolf DH, Rudolph HK. The medial-Golgi ion pump Pmr1 supplies the yeast secretory pathway with Ca^{2+} and Mn^{2+} required for glycosylation, sorting and endoplasmic reticulum-associated protein degradation. *Mol. Biol. Cell* 1998; **9**: 1149–1162.
44. Aoki I, Wu YJ, Silva AC, Lynch RM, Koretsky AP. *In vivo* detection of neuroarchitecture in the rodent brain using manganese-enhanced MRI. *Neuroimage* 2004; **22**: 1046–1059.